MILLIMETER ACCURACY SATELLITES FOR TWO COLOR RANGING

John J. Degnan
Code 901
NASA Goddard Space Flight Center
Greenbelt, MD 20771 USA

ABSTRACT

The principal technical challenge in designing a millimeter accuracy satellite to support two color observations at high altitudes is to provide high optical cross-section simultaneously with minimal pulse spreading. In order to address this issue, we provide, in this paper, a brief review of some fundamental properties of optical retroreflectors when used in spacecraft target arrays, develop a simple model for a spherical geodetic satellite, and use the model to determine some basic design criteria for a new generation of geodetic satellites capable of supporting millimeter accuracy two color laser ranging. We find that increasing the satellite diameter provides: (1) a larger surface area for additional cube mounting thereby leading to higher cross-sections; and (2) makes the satellite surface a better match for the incoming planar phasefront of the laser beam. Restricting the retroreflector field of view (e.g. by recessing it in its holder) limits the target response to the fraction of the satellite surface which best matches the optical phasefront thereby controlling the amount of pulse spreading. In surveying the arrays carried by existing satellites, we find that European STARLETTE and ERS-1 satellites appear to be the best candidates for supporting near term two color experiments in space.

1 INTRODUCTION

A companion article in these proceedings [Degnan, 1992] demonstrates the benefits of utilizing and maintaining ultrashort pulsewidths in performing two color ranging measurements to satellites. Unfortunately, even if one starts with a very short pulsewidth (e.g. 35 psec), most of the existing satellites will broaden the pulse significantly thereby degrading the precision of the differential time-of-flight measurement. This is especially true for the high altitude satellites, such as LAGEOS and ETALON, which are the primary targets for space geodesy applications. The principal technical challenge in designing a millimeter accuracy satellite to support two color observations at high altitudes is to provide high optical cross-section simultaneously with minimal pulse spreading. In order to address this issue, we provide, in this paper, a brief review of some fundamental properties of optical retroreflectors when used in spacecraft target arrays, develop a simple analytical model for spherical geodetic satellites, and use the model to determine some basic design criteria for a new generation of geodetic satellites capable of supporting millimeter accuracy two color laser ranging.

2 RETROREFLECTOR CHARACTERISTICS

For normally incident light, a single unspoiled retroreflector has a peak (on-axis) optical cross-section σ_{cc} defined by

$$\sigma_{cc} = \rho A_{cc} \left(\frac{4\pi A_{cc}}{\lambda^2} \right) \tag{2.1}$$

where ρ is the cube corner reflectivity, $A_{cc} = \pi R_{cc}^2$ is the light collecting area of the corner cube, and $4\pi A_{cc}/\lambda^2$ is the on-axis retroreflector gain. For a circular entrance aperture, the far field diffraction pattern (FFDP) of the reflected wave is the familiar Airy function given by [Born and Wolf, 1975]

$$\sigma(x) = \sigma_{cc} \left(\frac{2 J_1(x)}{x} \right)^2 \tag{2.2a}$$

where

$$x = k R_{cc} \sin(\theta_1) \tag{2.2b}$$

The Airy pattern consists of a main central lobe surrounded by weak rings. The angular half-width from the beam center to the first null is given by the first nonzero root of the Bessel function J_1 which, with (2.2b), yields the formula

$$\theta_{null} = 1.22 \frac{\lambda}{D_{cc}} \tag{2.3}$$

where λ is the wavelength and $D_{cc} = 2 R_{cc}$ is the diameter of the retroreflector.

At arbitrary incidence angle, the area in (2.1) is reduced by the factor [Minott, 1974]

$$\eta(\theta_{inc}) = \frac{2}{\pi}(\sin^{-1}\mu - \sqrt{2}\mu\tan\theta_{ref})\cos\theta_{inc} \tag{2.4}$$

where θ_{inc} is the incident angle and θ_{ref} is the refracted angle determined by Snell's law, i.e.

$$\theta_{ref} = \sin^{-1}\left(\sin\frac{\theta_{inc}}{n}\right) \tag{2.5}$$

where n is the cube index of refraction. The quantity μ is given by the formula

$$\mu = \sqrt{1 - 2\tan^2\theta_{ref}} \tag{2.6}$$

Thus the peak optical cross-section in the center of the reflected lobe falls off as

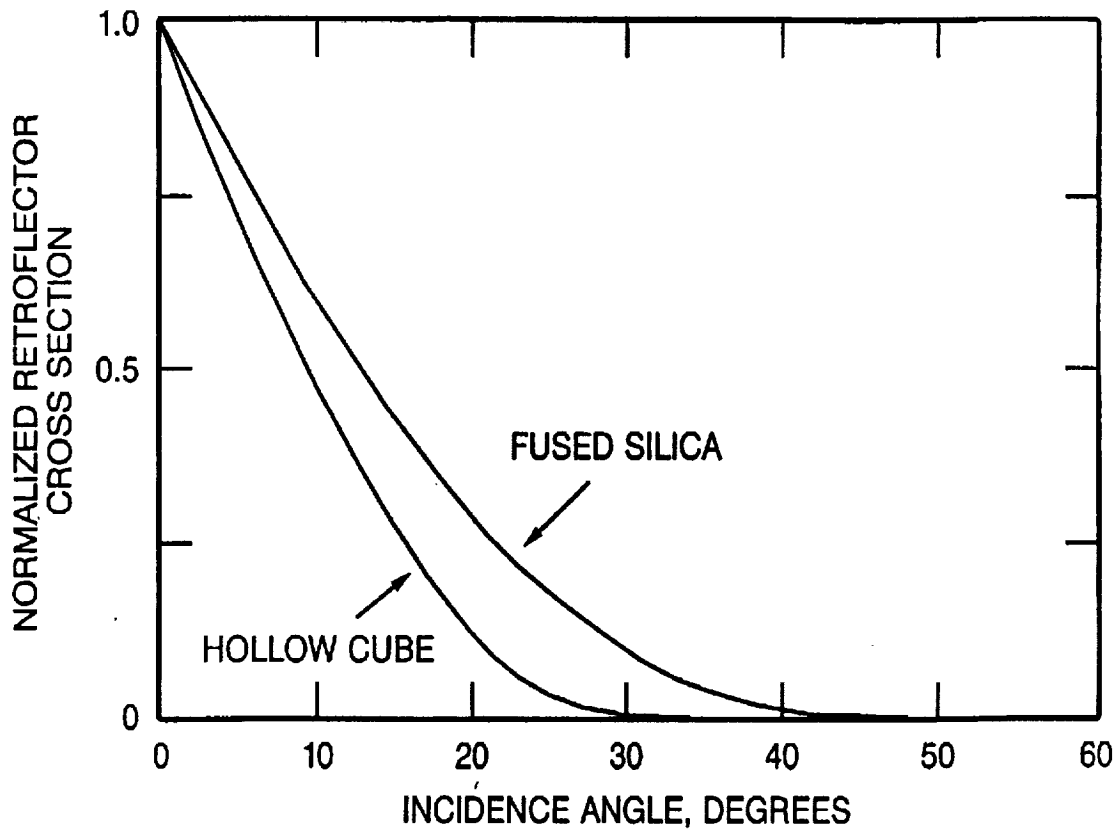$$\sigma_{eff}(\theta_{inc}) = \eta^2(\theta_{inc})\sigma_{cc} \tag{2.7}$$

Figure 1: Normalized peak optical cross-section as a function of incidence angle for an unspoiled retroreflector.

7-38

Figure 1 shows the falloff of optical cross-section with incidence angle for the two most common retroreflectors - hollow (n=1) and quartz (n=1.455). Note that, for a solid quartz cube, the optical cross-section falls to half its on-axis value at roughly 13° incidence angle and is effectively zero beyond about 40°. The cross-section for a hollow cube corner falls to half its normal incidence value at about 9° and is effectively zero beyond about 30°.

One can further limit the effective incidence angle over which the retroreflector responds by recessing the reflector in its holder. It can be easily shown that the incidence angle at which the retroreflector response is zero is given by

$$\theta_{max} = \cot^{-1}\left(\frac{d}{D_{cc}}\right) \tag{2.8}$$

where d is the depth of the recess.

3 VELOCITY ABERRATION

As mentioned previously, the far field diffraction pattern (FFDP) of a cube corner with a circular entrance pupil function corresponds to the familiar Airy pattern consisting of a single main lobe surrounded by low intensity rings. If there were no relative motion between the satellite and the target, the center of the FFDP would fall on the instantaneous line of sight between the target and satellite. However, due to the relative velocity between the satellite and the target, the coordinates of the FFDP are translated. The magnitude of the angular displacement in the FFDP is given by the equation [Minott, 1976]:

$$\alpha(h_s, \theta_{zen}, \omega) = \alpha_{max}(h_s)\sqrt{\cos^2\omega + \Gamma^2(h_s, \theta_{zen})\sin^2\omega} \tag{3.1}$$

where the maximum value, α_{max}, is given by the expression

$$\alpha_{max}(h_s) = \frac{2}{c}\sqrt{\frac{R_E^2 g}{R_E + h_s}} \tag{3.2}$$

and

$$\Gamma(h_s, \theta_{zen}) = \sqrt{1 - \left(\frac{R_E \sin\theta_{zen}}{R_E + h_s}\right)^2} \tag{3.3}$$

and R_E is the Earth radius, g = 9.8 m/sec² is the gravitational acceleration at the surface, h_s is the satellite height above sea level, c is the velocity of light, and the angle

$$\omega = \cos^{-1}[(\hat{r} \times \hat{\rho}) \cdot \hat{v}] \tag{3.4}$$

where $\hat{r}$, $\hat{\rho}$, and $\hat{\upsilon}$ are all unity length vectors corresponding to the satellite position vector (relative to the Earth center), the line-of-sight vector between station and satellite, and the satellite velocity vector respectively. Since $\Gamma(h_s, \theta_{zen})$ is always less than unity, equation (3.1) has an effective "minimum" value for a given θ_{zen}, when $\omega = \pi/2$. Thus,

$$\alpha_{min}(h_s, \theta_{zen}) = \alpha_{max}(h_s)\Gamma(h_s, \theta_{zen}) \qquad (3.5)$$

The maximum and minimum angular displacements of the FFDP are plotted as a function of satellite height in Figure 2 assuming a maximum θ_{zen} of 70°. It should be noted from the figure that the angular displacement decreases with altitude and that the maximum and minimum values converge for high satellites. At ETALON altitudes (19,000 Km), for example, the angular displacement is roughly constant at about 26 μrad.
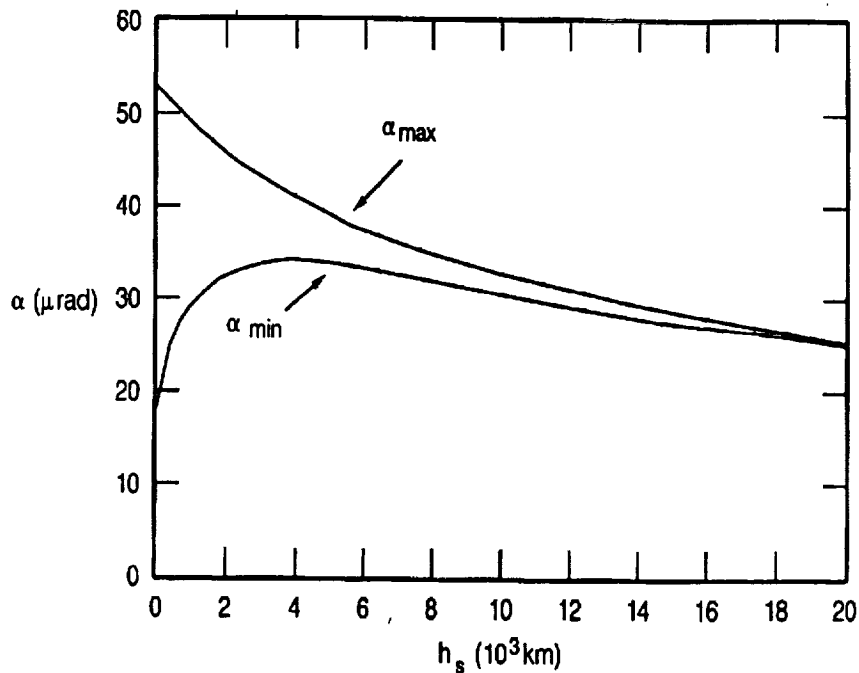
Figure 2: Maximum and minimum angular displacements in the retroreflector far field diffraction pattern caused by the velocity aberration effect as a function of satellite altitude above the Earth's surface.

If the target FFDP is angularly narrow relative to the size of the velocity aberration displacement, the receiver will lie on the low signal edge of the FFDP or even lie outside the FFDP entirely. For example, consider a moving retroreflector whose face is normal to the ranging system line-of-sight. The cross-section is given by (2.2a) with $x = kR_{cc}\sin(\alpha) \sim kR_{cc}\alpha$ where alpha is the instantaneous angular displacement caused by velocity

aberration. If $\alpha \ll \alpha_{null}$, the reduction in cross-section is negligible. However, if α is large, the reflected beam will "miss" the receiver and low or nonexistent signal levels will result. For non-normal incidence angles, the reflected FFDP is no longer circularly symmetric since the collecting (and transmitting) aperture of the retroreflector appears as an ellipse to the range receiver. The FFDP peak is again along the instantaneous receiver line-of-sight, but the FFDP is now given by the two-dimensional Fourier transform of the elliptic entrance aperture of the corner cube. The velocity aberration causes the retroreflector response to be reduced relative to the peak value given by (2.7). This reduction is greater for velocity vectors which are parallel to the long axis of the ellipse because of the faster falloff of the FFDP with angle in this direction.

4 RETROREFLECTOR "SPOILING"

To reduce the effects of velocity aberration in large retroreflectors, the retroreflector is often "spoiled". The goal of "spoiling" is to concentrate more reflected energy into the annular region bordered by α_{max} and α_{min}. Ideally, one would like to uniformly spread the energy within the annular ring yielding an optimum cross-section given by

$$\sigma_{ideal} = \rho A_{cc} \left(\frac{4\pi}{\Omega_{cc}} \right) = \rho A_{cc} \left(\frac{4}{\alpha_{max}^2 - \alpha_{min}^2} \right) \tag{4.1}$$

where the quantity in parentheses is the effective target gain and Ω_{cc} is the solid angle subtended by the annular ring of interest. However, conventional spoiling techniques generally result in average optical cross-sections which agree only within an order of magnitude with the ideal limit described by (4.1).

Spoiling is usually accomplished by introducing slight variations into the cube corner dihedral angles (typically less than two arcseconds). This creates a complicated FFDP which, for an incident beam normal to the cube face, breaks the initial single main Airy lobe into 2N lobes (where N = 1 to 3 is the number of spoiled dihedral angles) distributed within an angular annulus. The mean angular radius of the annulus increases linearly with the dihedral offset angle from a perfect cube and, from diffraction theory [see (2.3)], one expects the effective width of the various lobes to depend inversely on cube diameter.

Each of the 2N lobes originates from a different sector of the retroreflector entrance aperture. In fact, the FFDP of each lobe is determined by the two-dimensional Fourier transform of the projection of the 180°/2N sector of the (assumed) circular retroreflector entrance aperture into a plane perpendicular to the line-of-sight between the satellite and the station. The distribution of energy within this "annulus" is therefore highly nonuniform. Furthermore, the effective area for each lobe is reduced to:

$$A_{eff} = \eta(\theta_{inc}) \frac{A_{cc}}{2N} \qquad (4.2)$$

Substituting the latter expression into (2.1), we obtain an approximate expression for the peak optical cross-section at the center of one of the 2N lobes for the spoiled retroreflector at arbitrary incidence angle

$$\sigma_{peak}(\theta_{inc}, N) = \eta^2(\theta_{inc}) \frac{\sigma_{cc}}{(2N)^2} \qquad (4.3)$$

One can also "spoil" the retroreflector by placing or grinding a weak lens onto the entrance face. This approach retains the single central lobe of the unspoiled cube corner while reducing its peak amplitude and spreading the energy over a wider solid angle, Ω. This yields a peak cross-section given by

$$\sigma_{lens} = \rho A_{cc} \left(\frac{4\pi}{\Omega} \right) \qquad (4.4)$$

and can be an effective approach when velocity aberrations are sufficiently small.

5 SATELLITE OPTICAL CROSS-SECTION

As noted previously, the optical cross-section which can be achieved with a single retroreflector is limited by the need to compensate for velocity abberation effects. Received SLR signals can only be enhanced by summing the contributions of several retroreflectors. Modern geodetic target satellites (e.g., STAR-LETTE, LAGEOS, and ETALON) are all designed to be spherical in shape in order to avoid the large pulse spreading caused by earlier flat panel arrays when viewed at non-normal incidence. The spherical shape also simplifies the modelling of nonconservative forces acting on the satellite.

Satellite array size is largely determined by the satellite altitude since more retroreflectors are required to achieve reasonable signal-to-noise ratios over longer slant ranges. Thus, STARLETTE (960 Km), LAGEOS (5900 Km), and ETALON (19,200 Km) have diameters of 12, 60, and 129.4 cm and average optical cross-sections of .65, 7, and 60 million square meters respectively.

Let us consider a spherical satellite which is uniformly covered with retroreflectors. The density of cube corners, as a function of incidence angle, is easily seen to be

$$N(\theta_{inc}) d\theta_{inc} = \frac{N}{2} \sin\theta_{inc} d\theta_{inc} \qquad (5.1)$$

where N is the total number of reflectors on the satellite. To obtain a simple expression for the overall target cross-section σ, we approximate the sum over all of the retroreflectors within the allowed range of incidence angle by the following integral

$$\sigma = \sigma_{cc} \int_0^{\frac{\pi}{2}} d\theta_{inc} N(\theta_{inc}) \eta^2(\theta_{inc}) \qquad (5.2)$$

where we have used (2.7). If the retroreflectors are not recessed in their holders, $\eta(\theta_{inc})$ is given by (2.4). If their angular response is limited by the recess, the variation can be well-approximated by the expression

$$\eta(\theta_{inc}) = 1 - \frac{\theta_{inc}}{\theta_{max}} \qquad (5.3)$$

where θ_{max} is given by (2.8). Actually, (5.3) is an excellent approximation to (2.4) as well provided we choose θ_{max} equal to .54 rad (31°) for hollow cubes or .75 rad (43°) for solid cubes respectively (see Figure 1). Substituting (5.2) and (5.3) into (5.2) and evaluating the resulting integrals yields

$$\sigma = \frac{\sigma_{cc} N}{2} \left[1 - \frac{\sin^2\left(\frac{\theta_{max}}{2}\right)}{\left(\frac{\theta_{max}}{2}\right)^2} \right] \qquad (5.4)$$

Let us now examine the validity of (5.4) by substituting LAGEOS values. The LAGEOS satellite has a radius R = 29.8 cm and is imbedded with 426 retroreflectors (422 fused quartz and 4 germanium) with a clear aperture diameter D_{cc} of 3.81 cm. Ignoring the fact that four cubes are germanium, we choose N = 426 and a value of θ_{max} = .75 rad for solid quartz cubes. We now use a value σ_{cc} = 2.834 x 10⁶ in agreement with the input values to the RETRO computer program as determined during LAGEOS testing and evaluation [Fitzmaurice et al, 1977]. Substituting the latter values into (5.4) yields

$$\sigma_{LAGEOS} = 9.8 \sigma_{cc} = 2.78 x 10^7 m^2 \qquad (5.5)$$

This is roughly equal to the peak value computed by the much more detailed RETRO program which showed a range of values between .54 and 2.7 x 10⁷ m². Equation (5.4) tends to overestimate the actual cross-section because it includes only geometric, and not velocity aberration, effects. Equation (5.5) also implies that the LAGEOS array cross-section is roughly 9.8 times that of a single cube corner at normal incidence.
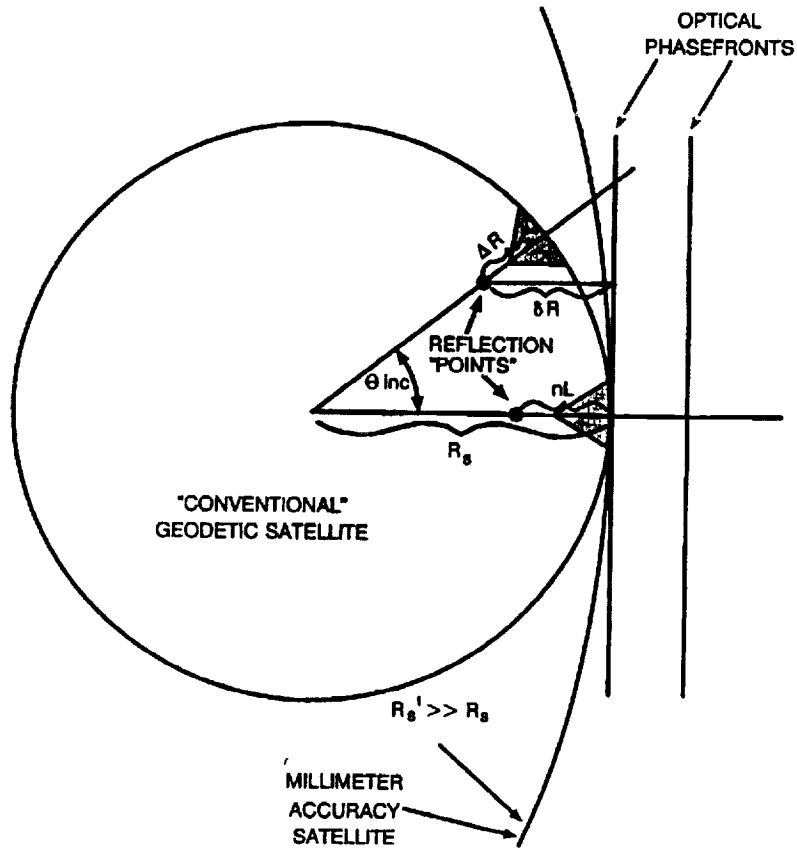
Figure 3: Diagram of a spherical geodetic satellite defining the variables used in the analysis.

6 SATELLITE IMPULSE RESPONSE AND TARGET SPECKLE

An individual retroreflector responds as a point source and hence does not spread the laser pulse in time. However, with a typical array of retroreflectors, the laser pulse arrives at the "reflection center" of each retroreflector at a slightly different time leading to a broadening of the received pulse [Degnan, 1985]. The location of the "reflection center" for an individual solid cube corner reflector is given by [Fitzmaurice et al, 1977; Arnold, 1978]

$$\Delta R(\theta_{inc}) = nL\sqrt{1 - \left(\frac{\sin\theta_{inc}}{n}\right)^2} = nL\cos\theta_{ref} \tag{6.1}$$

where $\Delta R(\theta_{inc})$ is measured from the center of the front face of the cube corner to the reflection point, L is the vertex to front face dimension, n is the refractive index of the corner cube material, θ_{inc} is the angle of incidence, and θ_{ref} is the corresponding refraction angle. From Figure 3, it can be seen that a

7-44

cube at an angle θ_{inc} to the incident wave produces a time delay, relative to the surface of the satellite closest to the ranging station ($\theta_{inc} = 0$), given by

$$\Delta t(\theta_{inc}) = \frac{2}{c}\{R_s - [R_s - \Delta R(\theta_{inc})]\cos\theta_{inc}\} = \frac{2R_s}{c}\left\{1 - \cos\theta_{inc}\left[1 - \frac{nL}{R_s}\cos\theta_{ref}\right]\right\} \quad (6.2)$$

where R_s is the satellite radius. It should also be noted that the differential delay between target reflection points also introduces a random phase delay between individual reflectors. Thus, if the temporal profiles from multiple cubes overlap at the range receiver, the electric fields will interfere with each other in a random way from shot to shot resulting in target "speckle". On average, however, the return waveform from the satellite should behave as if each of the retroreflectors is an incoherent source. This was an implicit assumption in our derivation of target optical cross-section in Section 5.

In the same spirit, the time-averaged satellite impulse response can be estimated by summing the weighted (incoherent) returns from each of the retroreflectors. Using the simple model for a spherical satellite introduced in Section 5, the impulse response can be shown to be

$$I(t) = \sigma_{cc}\frac{N}{2}\int_0^{\frac{\pi}{2}} d\theta_{inc}\sin\theta_{inc}\eta^2(\theta_{inc})\delta[t - \Delta t(\theta_{inc})] \quad (6.3)$$

where the geometric weighting factor is given by (2.4) or (5.3), $\Delta t(\theta_{inc})$ is given by (6.2), and the delta function $\delta[t - \Delta t(\theta_{inc})]$ represents an infinitely short laser pulse waveform incident on the satellite. From (6.2), we see that the delta function is nonzero only when the condition

$$\cos\theta(\tau,\epsilon,n) = \frac{1 - \tau}{1 - \epsilon\sqrt{1 - \frac{1}{n^2} + \left[\frac{\cos\theta(\tau,\epsilon,n)}{n}\right]^2}} \quad (6.4)$$

holds where we have defined the new variables

$$\tau = \frac{ct}{2R_s} \qquad\qquad \epsilon < \tau < \tau_{max}$$

$$\epsilon = \frac{nL}{R_s} \qquad \tau_{max} = 1 - \cos\theta_{max}\left[1 - \epsilon\sqrt{1 - \frac{1}{n^2} + \left(\frac{\cos\theta_{max}}{n}\right)^2}\right] \quad (6.5)$$

The variable τ is a normalized time, expressed in units of the roundtrip transit time from the surface of the satellite to the center and back, and ϵ is the ratio of the optical depth of the cube to the satellite radius. The minimum and maximum values of τ

are determined by setting θ equal to zero and θ_{max} respectively in (6.4) and solving for τ. The total pulse duration, measured at the baseline, is given by $\Delta t = t_{max} - \epsilon$.

From (5.3) and (6.3), the satellite impulse response can now be expressed as a function of the variables τ, ϵ, n, and θ_{max}, i.e.

$$I(\tau,\epsilon,n,\theta_{max}) = \sigma_{cc}\frac{N}{2}\sin\theta(\tau,\epsilon,n)\left[1 - \frac{\theta(\tau,\epsilon,n)}{\theta_{max}}\right]^2 \tag{6.6}$$

where $\theta(\tau,\epsilon,n)$ is defined by (6.4). In the limit of large satellite diameters ($\epsilon \to 0$), (6.4) reduces to the simple form

$$\theta(\tau,0,n) = \cos^{-1}(1-\tau) \tag{6.7}$$

and (6.6) becomes

$$I(\tau,0,n,\theta_{max}) = \sigma_{cc}N\sqrt{\frac{\tau}{2}\left(1-\frac{\tau}{2}\right)}\left[1 - \frac{\cos^{-1}(1-\tau)}{\theta_{max}}\right]^2 \tag{6.8}$$

The quantity ϵ is typically small and, for nonzero values of ϵ, (6.4) can be easily solved by iteration using (6.7) as a starting point, i.e.

$$[\cos\theta(\tau,\epsilon,n)]_{j+1} = \frac{1-\tau}{1-\epsilon\sqrt{1-\frac{1}{n^2}+\left[\frac{[\cos\theta(\tau,\epsilon,n)]_j}{n}\right]^2}} \tag{6.9}$$

until it converges.

As an illustration, let us use (6.6) to estimate the impulse response of the LAGEOS satellite. Substituting n = 1.455 (fused silica), L= 1.905 cm, and R_S = 29.8 cm into (6.5b), we obtain a value ϵ = .093. We recall that, for solid cube corners, we can use a value θ_{max} = .75 rad. Now, using (6.6) and (6.9), we obtain the plot of the LAGEOS impulse response shown in Figure 4(a). The profile shows the characteristic fast rise and long tail of the LAGEOS response. Furthermore, if we compute a center-of-mass correction from the centroid of this impulse response profile, we obtain a value of 250.2 mm which is in excellent agreement with the accepted LAGEOS value of 249 ± 1.7 mm [Fitzmaurice et al, 1977].

The impulse response in the large satellite limit, given by (6.8), is shown in figure 4(b) for the case of solid quartz and hollow cubes. Note that both the temporal width of the reflected pulse and the target optical crossection is smaller for the hollow cubes than for the solid cubes because of their smaller field of view.
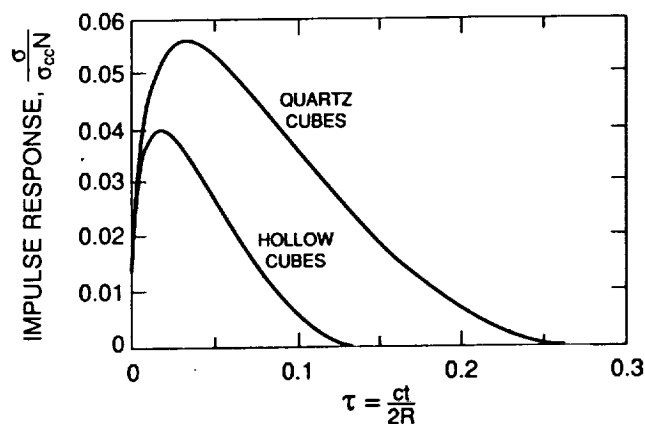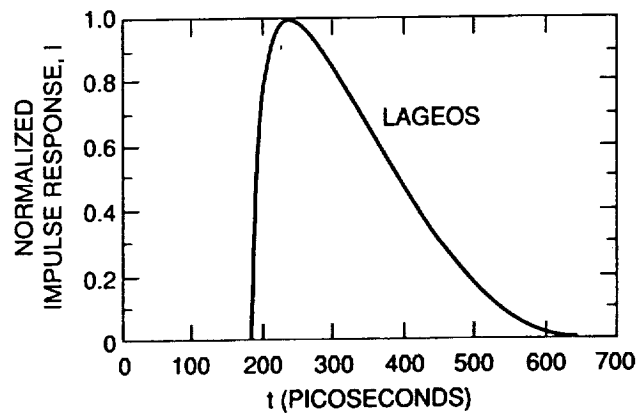
Figure 4: (a) Impulse response of the LAGEOS satellite as computed by our simple analytical model. (b) Impulse response in the large satellite limit for both hollow and solid quartz cubes.

7 FEASIBILITY OF MILLIMETER ACCURACY SATELLITES

We will now demonstrate that, in order to achieve high optical cross-section simultaneously with minimal pulse spreading with a spherical satellite, we must increase the satellite diameter and/or retroreflector density and simultaneously restrict the response to retroreflectors within a relatively small solid angle on the satellite surface about the station line of sight.

The total time duration of the reflected pulse (0% to 0% intensity points) can be determined from (6.5), i. e.

$$\Delta t = \frac{2R_s}{c}(\tau_{max} - \epsilon) = \frac{2R_s}{c}\left\{ 2\sin^2\frac{\theta_{max}}{2} + \epsilon\left[\cos\theta_{max}\sqrt{1 - \frac{\sin^2\theta_{max}}{n^2}} - 1 \right] \right\} \qquad (7.1)$$

which, in the limit of small maximum incidence angles, reduces to

$$\Delta t \sim \frac{R_s}{c}\theta_{max}^2\left[1 - \epsilon\left(1 + \frac{1}{n^2} \right) \right] \qquad (7.2)$$

In the same limit, Eq. (5.4) for the satellite optical cross-section reduces to

$$\sigma \sim \frac{\sigma_{cc}N}{24}\theta_{max}^2 \qquad (7.3)$$

As mentioned earlier, the angular response can be restricted by recessing the retroreflectors in their holders. Substituting (7.2) into (7.3) yields

$$\sigma = \frac{\sigma_{cc}N}{24}\frac{c\Delta t_{max}}{R_s\left[1 - \frac{nL}{R_s}\left(1 + \frac{1}{n^2} \right) \right]} \qquad (7.4)$$

We can now express the total number of retroreflectors as

$$N = 4\beta\frac{R_s^2}{R_{cc}^2} \qquad (7.5)$$

where β is a "packing density" (= .435 for LAGEOS) which represents the fraction of total surface area occupied by the cube faces. Substituting (7.5) into (7.4) yields our final result

$$\sigma \sim \frac{\sigma_{cc}}{6R_{cc}^2}\frac{\beta R_s c\Delta t}{\left[1 - \frac{nL}{R_s}\left(1 + \frac{1}{n^2} \right) \right]} \qquad (7.6)$$

The product $\beta R_s c\Delta t$ in (7.6) quantifies our earlier statement that, if we wish to reduce the amount of pulse-spreading Δt by some factor (via reduction of the retroreflector field-of-view), we must increase the retroreflector packing density -satellite radius product (βR_s) by the same factor to retain a similar target cross-section.

8 CONCLUSION

As mentioned previously, the principal technical challenge in designing a millimeter accuracy satellite to support two color observations at high altitudes is to provide high optical cross-section simultaneously with minimal pulse spreading. Increasing the satellite diameter provides: (1) a larger surface area for additional cube mounting thereby leading to higher cross-sections; and (2) makes the satellite surface a better match for

the incoming planar phasefront of the laser beam as in Figure 3. Simultaneously restricting the retroreflector field of view (e.g. by recessing it in its holder) limits the target response to the fraction of the satellite surface which best matches the optical phasefront thereby reducing the amount of pulse spreading.

For near term experiments, the small radius of STARLETTE makes it an attractive target for testing and evaluating two color systems or for testing atmospheric models. Furthermore, its low altitude (960 Km) and moderate target cross section results in relatively high received signal levels. AJISAI, also in a relatively low 1375 Km orbit, consists of small clusters of retroreflectors separated by large reflecting panels and has comparable signal strength to STARLETTE. Unfortunately, the satellite is quite large and simultaneous returns from several retro clusters results in a complicated satellite signature [Prochazka et al, 1991]. From Figure 4, LAGEOS spreading is in excess of 150 picoseconds FWHM in agreement with [Fitzmaurice et al, 1977] although, with sufficiently short laser pulses (<50 psec), individual retro rings should be resolvable via streak cameras at certain satellite orientations. (Note that the simple satellite model presented here gives an average response over the full range of satellite orientations and shows none of the structure expected from a particular orientation). The LAGEOS pulse spreading combined with relatively low signal returns, measured at the few to several tens of photoelectron level for most systems, would make the necessary differential timing very difficult [Degnan, 1992].

Another useful target for two-color system evaluation is the recently launched European Earth Remote Sensing satellite, ERS-1. It flies at a relatively low altitude (<800 Km) and has a small compact target consisting of one nadir-viewing retroreflector surrounded by a uniformly spaced ring of eight identical cube corners at a nadir angle of 50°. Approximate modelling of this satellite by the author indicates that sharp returns consisting of one or two peaks (well separated) can be obtained from most viewing angles as illustrated in Figure 5. At nadir angles between 0° and 15°, the nadir viewing cube is dominant whereas, for nadir angles between 30° and 70°, the ring provides a sharp return at virtually all azimuthal angles. At nadir angles between about 15° and 30°, there is some overlapping of returns and pulse distortion.
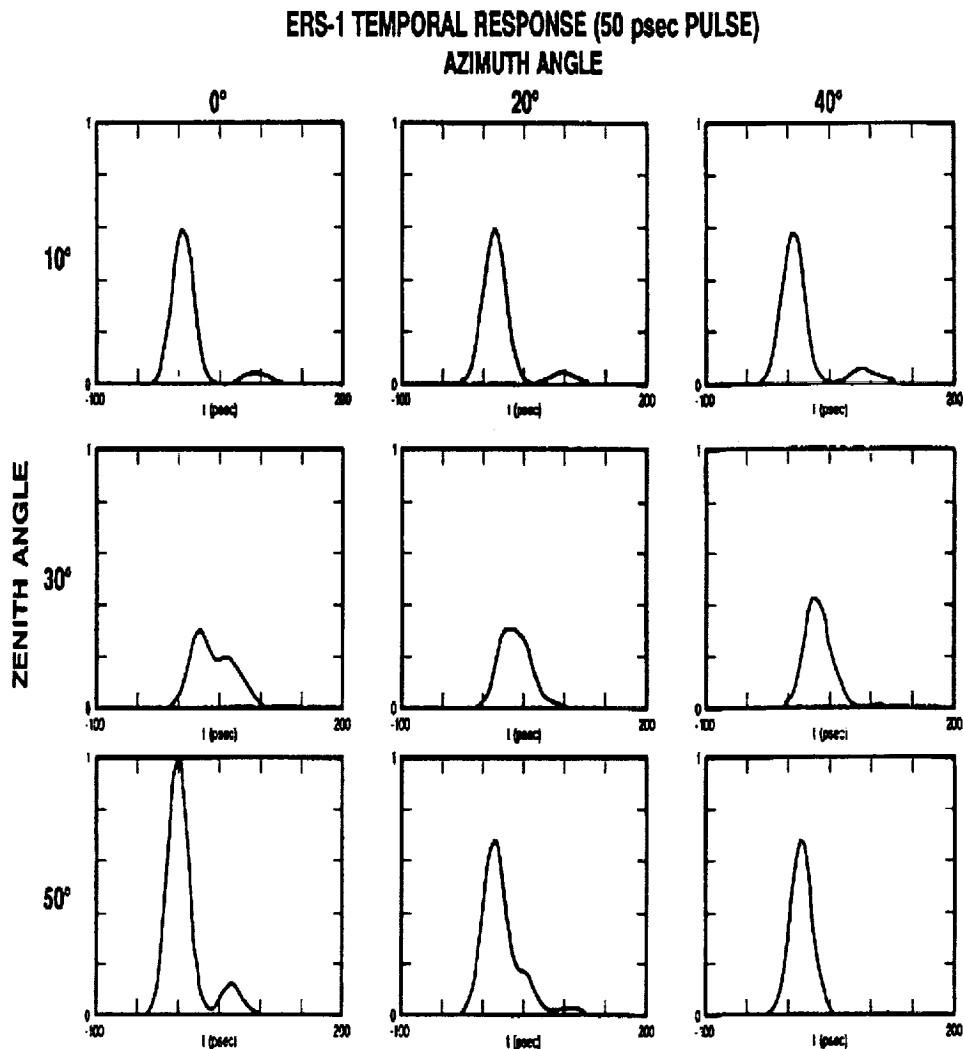
Figure 5: Approximate (geometric) response of the ERS-1 satellite to a 50 picosecond pulse as a function of nadir and azimuthal angle.

9 REFERENCES

Arnold, D. A., "Optical and infrared transfer function of the LAGEOS retroreflector array", Final Report NASA Grant NGR 09-015-002, Smithsonian Institution Astrophysical Observatory, May 1978.

Born M. and E. Wolf, "Principles of Optics", Chapter 8, Pergamon Press, New York, 1975.

Degnan, J. J., "Satellite laser ranging: current status and future prospects", IEEE Trans. on Geoscience and Remote Sensing, GE-23, pp. 398-413, 1985.

Degnan, J. J., "Optimum wavelengths for two color ranging", these proceedings, May 1992.

Fitzmaurice, M. W., P. O. Minott, J. B. Abshire, and H. E. Rowe, "Prelaunch testing of the Laser Geodynamic Satellite (LAGEOS)", NASA Technical Paper 1062, October 1977.

Minott, P. O., "Design of retrodirector arrays for laser ranging of satellites", NASA TM-X-723-74-122, Goddard Space Flight Center, March, 1974.

Minott, P. O., "Reader's Guide to the RETRO Program Output", NASA TM-X-722-76-267, Goddard Space Flight Center, September, 1976.

Prochazka, I., K. Hamal, G. Kirchner, M. Schelev, and V. Postovalov, "Circular streak camera application for satellite laser ranging", presented at SPIE Conference on Electronic Imaging, San Jose, California, Feb. 24-27, 1991.